ADVANCES IN ATMOSPHERIC SCIENCES, VOL. 25, NO. 1, 2008, 1–10

Absorption Properties of Urban/Suburban Aerosols in China

QIU Jinhuan*[1,2] (邱金桓) and YANG Jingmei (杨景梅)

Laboratory for Middle Atmosphere and Global Environment Observation (LAGEO), Institute of Atmospheric Physics, Chinese Academy of Sciences, Beijing 100029

(Received 4 December 2006; revised 21 May 2007)

ABSTRACT

The broadband diffuse radiation method is improved to retrieve the aerosol refractive index imaginary part (AIP) and broadband (400–1000 nm mean) single scattering albedo (SSA). In this method, four sets of SSA selection criteria are proposed for quality control. The method is used to retrieve AIP, SSA and absorptive optical thickness (AbOT) from routine hourly-exposed pyrheliometer and paranometer measurements over 11 sites (meteorological observatories) in China during 1998–2003. Apart from one suburban site (Ejin Qi), the other urban sites are all located around big or medium cities. As shown in the retrieval results, annual mean SSA during 1998–2003 changes from 0.941 (Wuhan) to 0.849 (Lanzhou), and AIP from 0.0054 to 0.0203. The 11-site average annual mean SSA and AIP are 0.898 and 0.0119, respectively. SSA during winter is smaller for most sites. There is an evidently positive correlation between SSA and aerosol optical thickness (AOT) for all sites. There is also a positive correlation between SSA and relative humidity for most sites, but a negative correlation for a few sites, such as Kashi and Ürümqi in Northwest China.

Key words: broadband radiation method, aerosol, single scattering albedo, imaginary part, correlative coefficient

DOI: 10.1007/s00376-008-0001-0

1. Introduction

Atmospheric aerosols are receiving more and more attention in studies of radiative forcing (Charlson et al., 1992; Kiehl and Briegleb, 1993; Penner et al., 1994; Taylor and Penner, 1994; Bengtsson et al., 1999; Menon et al., 2002). Aerosols are also very important in the atmospheric correction of satellite remote sensing (Kaufman et al., 1997). Sulfate aerosols, carbonaceous aerosols and mineral dust have a substantial radiative forcing in a cloud-free atmosphere. It is comparable with the effect of greenhouse gases (Charlson et al., 1992; Kiehl and Briegleb, 1993; Penner et al., 1994). These estimates are, however, still quite uncertain in quantity (Kiehl and Briegleb, 1993; Taylor and Penner, 1994; Tegen et al., 1996). In particular, a lack of information on aerosol absorption is significant (Penner et al., 1994). The same obstacle exists in the atmospheric correction of space-borne remote sensing, which is limiting scientists from obtaining accurate information from satellite data. In addition, recent research presented by Menon et al. (2002) shows very significant climate effects of strongly-absorbing black carbon aerosols in China and India. In their climate model, single scattering albedo (SSA), a key input parameter, is assumed as 0.85 for aerosols in China. By now the true SSA information is far from adequate. Therefore, improving this information will increase our knowledge on aerosol absorption, which is significant for estimating aerosol radiative forcing.

There is a large amount of routine observation data of broadband solar global/direct/diffuse radiation available worldwide. Based on this fact, some authors have attempted to develop methods using broadband solar radiation for AIP and SSA retrievals (Nakajima et al., 1996; Wei and Qiu, 1998; Qiu et al., 2004; Qiu, 2006). In the broadband diffuse radiation method (BRM), proposed by Qiu et al. (2004), first the broadband diffuse radiation is determined from both pyrheliometer and paranometer data, and then AIP and 1-μm-wavelength SSA are retrieved from the radiation. As shown in some studies (Dubovik et al., 2002; Eck et al., 2005) by using the Aerosol Robotic Network (AERONET) database (Holben et al., 1998), aerosol

*Corresponding author: QIU Jinhuan, jhqiu@mail.iap.ac.cn

SSA is closely wavelength dependent. The AERONET SSA product covers the spectrum from 440–1020 nm. In order to match with the AERONET SSA product, a method to retrieve 440–1020 nm broadband SSA from broadband solar radiation is proposed in this paper. Furthermore, the method is used to retrieve SSA and AIP from broadband radiation data over 11 sites in China, and the SSA properties are vigorously analyzed.

2. Methodology

In this section, the AIP and broadband SSA retrieval method, and the absorptive optical thickness (AbOT) determination approach are presented.

2.1 *AIP and SSA retrievals and their selection criteria*

In the broadband diffuse radiation method proposed by Qiu et al. (2004), there are four retrieval steps: (1) 750-nm aerosol optical thickness (AOT) retrieval from pyrheliometer data using the broadband extinction method (Qiu, 2001, 2003); (2) broadband diffuse radiation determination from both pyrheliometer and paranometer data; (3) AIP retrievals from diffuse radiation under assumptions of Junge-type aerosol size distribution and wavelength-independent AIP; (4) 1 μm-wavelength SSA determination using the AIP from step 3 and according to the Mie scattering calculation. This method is developed to retrieve AIP and broadband (λ, 440–1020 nm) SSA from broadband diffuse radiation. Broadband SSA($\omega_{\rm Broad}$) is defined as:

$$\omega_{\rm Broad} = \frac{l}{\lambda_2 - \lambda_1} \int_{\lambda_1=440}^{\lambda_2=1020} \omega(\lambda) d\lambda \,. \qquad (1)$$

In the present method, to retrieve $\omega_{\rm Broad}$ the first three steps are the same. The unique difference is the fourth step. In this step there are two tasks. First, the selection of different AIP and Ångtröm index (α) and building a library of $\omega_{\rm Broad}$ according to the Mie scattering calculations. And secondly, using the library to determine $\omega_{\rm Broad}$, corresponding to the AIP from the third step, which is regarded as the $\omega_{\rm Broad}$ solution.

The broadband radiation method demands some assumptions, such as Junge-type aerosol size distribution and wavelength-independent AIP. These assumptions, as well as radiation measurement error and cloud effect, can cause some uncertainty in AIP and SSA retrievals. In order to decrease the uncertainty, four sets of SSA selection criteria for quality assurance are proposed as follows:

(1) AOT and solar zenith angle cosine (μ_0) criteria

There may be a large error in paranometer measurement when the solar zenith angle θ_0 is beyond 75°, due to cosine effect. Therefore, a constraint to the radiation data selection is $\theta_0 < 72.54°$ ($\mu_0 > 0.3$). The larger the aerosol optical depth (AOD) is, and the smaller the μ_0, the more sensitive to the AIP variation the diffuse radiation is (Herman et al., 1975; Wei and Qiu, 1998). Based on this fact, another constraint to the radiation data selection is $\tau_a/\mu_0 > 0.3$ where τ_a is the AOD at the wavelength of 0.75 μm..

(2) AIP range criterion

AIP usually falls between 0.005 and 0.02 (Paltridge and Platt, 1976). In this paper, AIP is constrained to the range 0 <AIP<0.08 and the data of AIP$\geqslant$0.08 are deleted.

(3) Cloud criteria

The diffuse radiation method for AIP and SSA retrievals is available in the case of a pure aerosol-loading (no cloud) atmosphere. Cloud can be a key factor affecting SSA retrieval accuracy. There are three cloud fraction ($C_{\rm f}$) records during the day (0800, 1400 and 2000 LST) at meteorological observatories in China. The real-time $C_{\rm f}$ is determined through interpolation among the three records, which is used to select radiation data. If the 0800 $C_{\rm f}$ record is equal to zero, the $C_{\rm f}$ before 0800 from the interpolation can be negative. For this reason, the 0800 $C_{\rm f}$ record is regarded as the $C_{\rm f}$ before 0800. Only radiation data without any cloud cover ($C_{\rm f} = 0$) are taken in the AIP/SSA retrievals. According to this constraint criterion, data before 1400 can be selected only in the case of zero $C_{\rm f}$ records at 0800 and 1400. Because of no real-time cloud fraction measurement and usually great cloud variation in time and space, three zero records cannot justify zero cloud cover during 0800–2000. Cloud contribution to column total optical thickness can result in an overestimated aerosol scaling height ($Z_{\rm a}$) determination (Qiu, 2003; Qiu et al., 2005). So, another criterion to weaken cloud effect is the constraint that $Z_{\rm a}$ must be within three times of the monthly mean $Z_{\rm a}$.

(4) Standard deviation criterion

Defining a standard deviation criterion, SSA retrievals with a larger deviation to their mean values are omitted. The SSA and AIP data, in accordance with the above three constraint selections, are used to calculate the mean value and the standard deviation (σ). If σ is larger than a given value (marked as σ_0), the SSA with the maximum deviation to the mean SSA is deleted. This procedure will continue until σ is smaller than σ_0. $\sigma_0 = 0.05$ is taken in this paper.

Available SSA data in winter are often much larger than those in other seasons, and thus annual mean SSA from all SSA data may dominantly indicate the SSA during winter. For this reason, four seasonal mean SSA datasets are averaged to yield the annual mean SSA. As shown in the study by Qiu et al. (2004), if

errors in radiation measurements, relative aerosol parameters and water vapor amount inputs are random, the mean SSA and AIP from a large number of retrievals are much more reliable. In order to increase the data amount, annual/seasonal mean SSA and AIP during 1998–2003 are estimated. In addition, December, January and February are regarded as winter; March, April and May are spring; June, July and August are summer; September, October and November are autumn.

2.2 *AbOT determination*

As presented above, SSA retrievals with a smaller AOT are omitted, in which there may be a larger SSA uncertainty. As a result, the AOT averaged from all AOT data may be evidently smaller than the mean AOT from the AOT data having a simultaneously available SSA source, and an overestimated AbOT mean can be obtained if only the data having both AOT and SSA sources are used to determine the AbOT. Now, the mean AbOT is given by:

$$\tau_{\mathrm{Ab,mean}} = \frac{l}{N}\sum_{i=1}^{N}\tau_{\mathrm{a},i}(1-\omega_{\mathrm{a},i})\ , \qquad (2)$$

where N is the total AOT data number, and $\tau_{\mathrm{a,i}}$ and $\omega_{\mathrm{a},i}$ are the ith AOT and SSA, respectively. When both AOT and SSA are available, the SSA is an input. When SSA retrieval is unavailable, the SSA averaged using all SSA data is used to calculate AbOT. The AOT is usually smaller in the case without unavailable SSA retrieval, and so a weak effect of this approximation on total mean AbOT determination is estimated.

3. Aerosol absorption properties of over 11 urban/suburban sites

This section focuses on four areas: (1) sites and data studied; (2) comparison of BRM SSA with AERONET SSA; (3) annual/seasonal mean aerosol absorption properties; and (4) relationships between SSA with AOT and surface relative humidity (RH).

3.1 *Sites and data*

Figure 1 shows the 11 sites (first-class meteorological observatories) used in this study. Apart from Ejin Qi, which is a suburban site, all other sites (Shenyang, Beijing, Ürümqi, Golmud, Kashi, Lanzhou, Zhengzhou, Wuhan, Shanghai, and Chengdu) are located around large- or medium-sized cities. All AIP/SSA retrievals use hourly-exposed pyrheliometer and paranometer data in these sites during 1998–2003. The radiation instruments are calibrated once every two years, using international standard instruments. The pyranometer and pyrheliometer have, respectively, 5% and 2% calibration accuracy, as well as 5% and 2% annual stability (CMA, 1996). The AIP and SSA retrievals demand the input of surface water vapor pressure, visibility and cloud fraction. There are four daily records of cloud cover, surface visibility and water vapor pressure at meteorological observatories in China, made at 0200, 0800, 1400, and 2000 LST. Their values at other times are obtained from the last three records through linear interpolation.

3.2 *Comparison of BRM SSA with AERONET SSA*

Figure 2 illustrates a comparison of the hourly mean broadband (440–1020 nm) BRM SSA at the Beijing site with the dually-averaged AERONET SSA. The first average (marked as ω_0 of four AERONET real-time SSA datasets at wavelengths (λ_i) of 440, 670, 870, and 1020 nm, is given by:

$$\omega_0 = \frac{l}{\lambda_4-\lambda_1}\sum_{i=1}^{3}[\omega(\lambda_{i+1})+\omega(\lambda_i)](\lambda_{i+1}-\lambda_i)/2\ . \qquad (3)$$

Then, all ω_0 data during a one-hour period of broadband radiation observation are averaged to yield the mean SSA for its comparison with BRM SSA. There is usually one AERONET SSA retrieval during the one-hour period. The broadband radiation site is about 14 km away from the AERONET site. The comparable SSA data meet two conditions: (1) both SSA sources are available; and (2) there is at least one time of AERONET measurement during the one-hour broadband radiation observation. There are a total of 89 sets of comparative SSA data during 2001–2003. As shown in Fig. 2, the standard deviation between BRM SSA and AERONET SSA is 0.044, and their maximum deviation is 0.092. The mean AERONET SSA and BRM SSA are 0.877 and 0.897 with the 0.02 deviation, respectively. It is noted that there is a considerable oscillation deviation between both SSA data, partly caused by random errors of radiation data and input aerosol parameters (Qiu et al., 2004). Furthermore, we compared BRM AIP retrievals with AERONET AIP (Level-2.0), averaged by using a similar method as in Eq. (3). There are a total of 99 sets of comparative AIP data during 2001–2003. The mean AERONET AIP and BRM AIP are 0.014 and 0.0113 with a 0.0027 deviation, respectively, and the standard deviation between them is 0.0069.

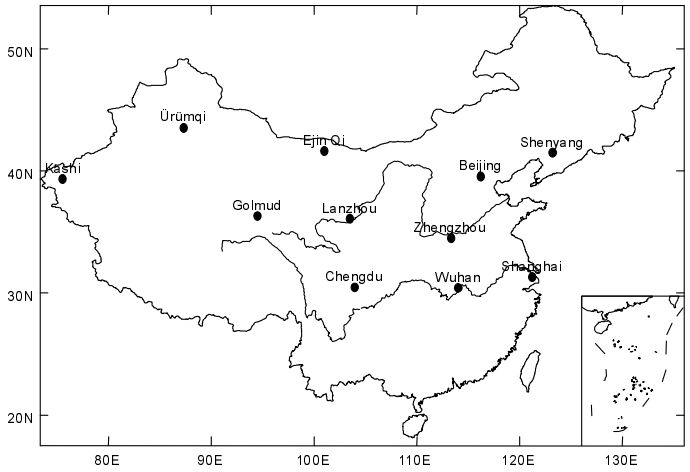

Fig. 1. Map of the 11 sites (meteorological observatories) used in this study.

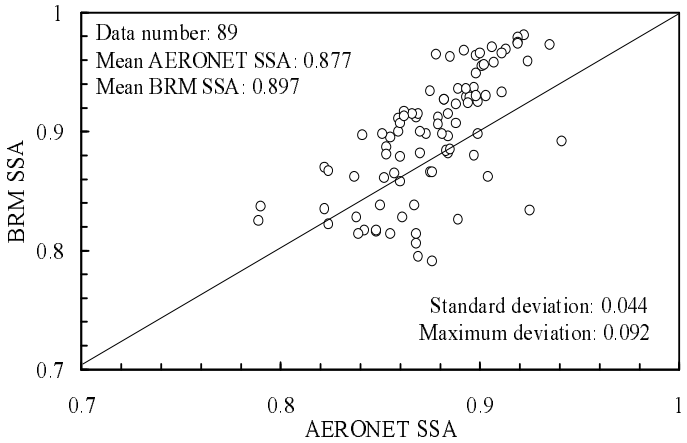

Fig. 2. Comparison of the hourly mean BRM SSA with AERONET SSA during 2001–2003.

Table 1. Total SSA data numbers.

Site	Whole year	Winter	Spring	Summer	Autumn
Shenyang	1331	485	343	153	345
Beijing	2194	664	693	350	481
Ejin Qi	477	47	186	185	51
Ürümqi	2166	577	585	277	710
Kashi	1772	239	377	394	756
Golmud	521	75	215	158	69
Lanzhou	2842	932	559	534	790
Zhengzhou	2208	606	697	188	705
Shanghai	984	363	260	145	216
Wuhan	1240	468	228	48	496
Chengdu	222	49	115	15	35

Table 2. Annual/seasonal mean SSA.

Site	Whole year	Winter	Spring	Summer	Autumn
Shenyang	0.881	0.87	0.878	0.903	0.889
Beijing	0.890	0.867	0.906	0.907	0.888
Ejin Qi	0.902	0.920	0.898	0.907	0.901
Ürümqi	0.889	0.882	0.898	0.896	0.887
Kashi	0.920	0.930	0.924	0.912	0.920
Golmud	0.890	0.906	0.891	0.887	0.884
Lanzhou	0.849	0.837	0.848	0.860	0.857
Zhengzhou	0.916	0.895	0.924	0.928	0.927
Shanghai	0.901	0.878	0.918	0.928	0.902
Wuhan	0.941	0.927	0.947	0.962	0.950
Chengdu	0.902	0.877	0.911	0.926	0.924
Total mean	0.898	0.890	0.904	0.911	0.903

Table 3. Annual/seasonal mean AIP.

Site	Whole year	Winter	Spring	Summer	Autumn
Shenyang	0.0145	0.0164	0.0149	0.0109	0.0131
Beijing	0.013	0.0167	0.0105	0.0104	0.0134
Ejin Qi	0.0112	0.0085	0.0118	0.0105	0.0114
Ürümqi	0.0132	0.0143	0.0119	0.0122	0.0136
Kashi	0.0086	0.0072	0.0081	0.0098	0.0086
Golmud	0.013	0.0106	0.0128	0.0135	0.0139
Lanzhou	0.0203	0.0227	0.0205	0.0181	0.0187
Zhengzhou	0.0091	0.0123	0.0079	0.0076	0.0073
Shanghai	0.0113	0.015	0.0089	0.0073	0.0109
Wuhan	0.0054	0.0073	0.0047	0.0027	0.0042
Chengdu	0.011	0.0142	0.0096	0.0078	0.0077
Total mean	0.0119	0.0132	0.011	0.0101	0.0112

3.3 *Annual/seasonal mean aerosol absorption properties*

Table 1 shows the annual/seasonal total data numbers of available hourly mean SSA retrievals from the 11 sites during 1998–2003. The annual data number changes between 222 (Chengdu) and 2842 (Lanzhou). During summer, the available SSA data is usually less, and the minimum number is 15 for the Chengdu site, mainly due to often high cloud cover.

Figure 3 shows SSA data numbers in different SSA solution ranges over the Beijing (Fig. 3a) and Wuhan (Fig. 3b) sites during 1998–2003. As shown in Fig. 3a, the mean value of total 2764 SSA data is 0.882 in Beijing, 86.2% SSA data are in the 0.8–0.98 SSA range, and the maximum data number is within the 0.88–0.9 range. In the case of Wuhan, most SSA data concentrate in the 0.88–0.98 range, and correspondingly, the mean SSA is 0.941.

Table 2 and Table 3 provide annual/seasonal mean SSA and AIP in the 11 sites during 1998–2003. As shown in these tables, the annual mean SSA changes from 0.941 (Wuhan) to 0.849 (Lanzhou), and the AIP from 0.0054 to 0.0203. There is often a high surface level RH, with its mean value being 72.1% (see Table 5) in Wuhan. The SSA could have an increasing trend with increasing RH (Hartley et al., 2000), particularly for water-soluble aerosols. The high RH in Wuhan is considered to be a factor impacting significantly on the smallest AIP and largest SSA. The 11-site mean annual mean SSA and AIP are 0.898 and 0.0119, respectively. The 11-site mean seasonal mean SSA is 0.89, 0.904, 0.911, 0.903 for winter, spring, summer, and autumn, respectively. The SSA during winter is smaller for most sites.

As shown in Table 4, the annual mean AOT changes from 0.125 (Ejin Qi) to 0.657 (Chengdu), with a total mean value of 0.402, and the AbOT from 0.012 (Ejin Qi) to 0.071 (Lanzhou), with a total mean value of 0.038. The annual mean aerosol scaling height changes from 1.465 km (Ejin Qi) to 3.256 km (Wuhan), with a total mean value of 2.306 km.

3.4 *Relationships between SSA, AOT and surface RH*

There is often strong oscillatory variation of the retrieved SSA with AOT or RH, partly due to SSA re-

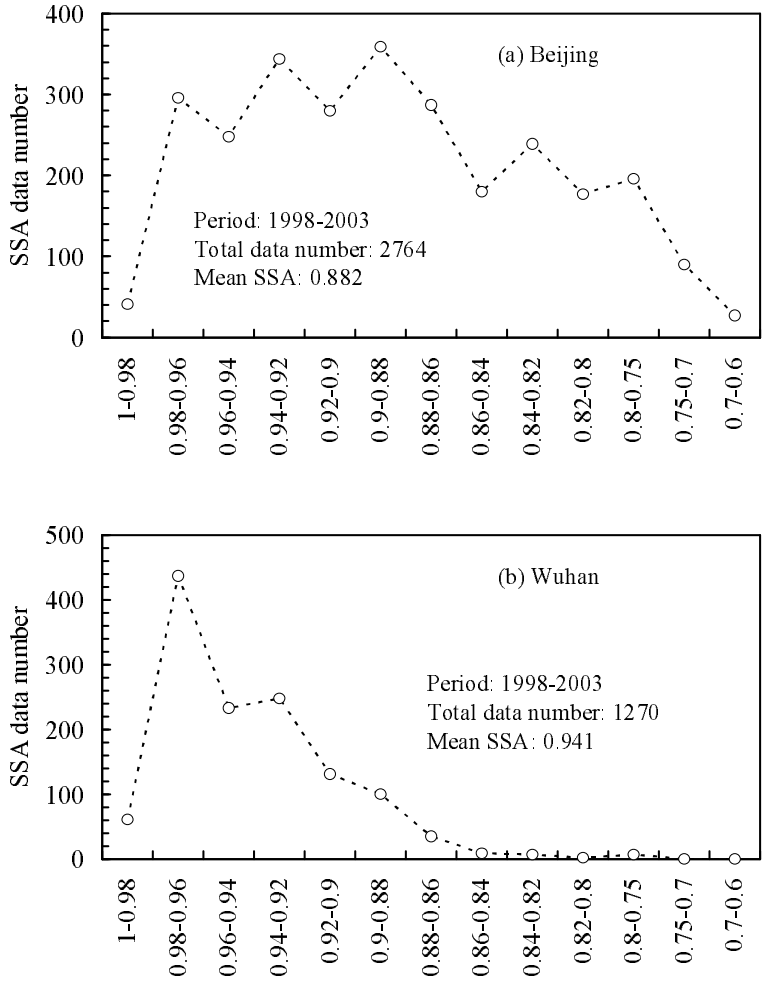

Fig. 3. SSA data numbers in different SSA ranges for (a) Beijing and (b) Wuhan.

Table 4. Annual mean 750-nm AOT, AbOT, and aerosol scaling height (Z_a).

Site	AOT	AbOT	Z_a (km)
Shenyang	0.383	0.044	1.601
Beijing	0.352	0.035	1.591
Ejin Qi	0.125	0.012	1.465
Urumqi	0.325	0.035	2.968
Kashi	0.386	0.029	2.735
Golmud	0.169	0.018	1.821
Lanzhou	0.49	0.071	2.878
Zhengzhou	0.538	0.041	1.842
Shanghai	0.487	0.043	2.727
Wuhan	0.515	0.029	3.256
Chengdu	0.657	0.061	2.475
Total mean	0.402	0.038	2.306

trieval uncertainty. In order to highlight the relationships between SSA and AOT or humidity, the AOT or humidity variation range is divided into a number of sub-ranges in calculating correlation coefficients between them. The sub-range number ($N_{\rm Range}$) and corresponding data number (N_0) in every sub-range are determined according to the following equations:

$$N_{\rm Range} = 4 + {\rm int}(N_{\rm total}/1000)\,, \tag{4}$$

$$N_{\rm Range} = 15, \ \text{when} \ N_{\rm Range} > 15\,, \tag{5}$$

$$N_0 = {\rm int}(N_{\rm total}/N_{\rm Range})\,, \tag{6}$$

where $N_{\rm total}$ is the total data number. The data number in every sub-range determined by using Eqs. (4)–(6) is almost uniform. The mean AOT and SSA in the sub-range are called sub-mean AOT and SSA. Next, relationships between sub-mean SSA and AOT or RH are analyzed according to Table 5 and Figs. 4–5.

As shown in Table 5, the correlation coefficient (η_1) between SSA and AOT is not less than 0.632 for all 11 sites, implying an evidently increasing variation

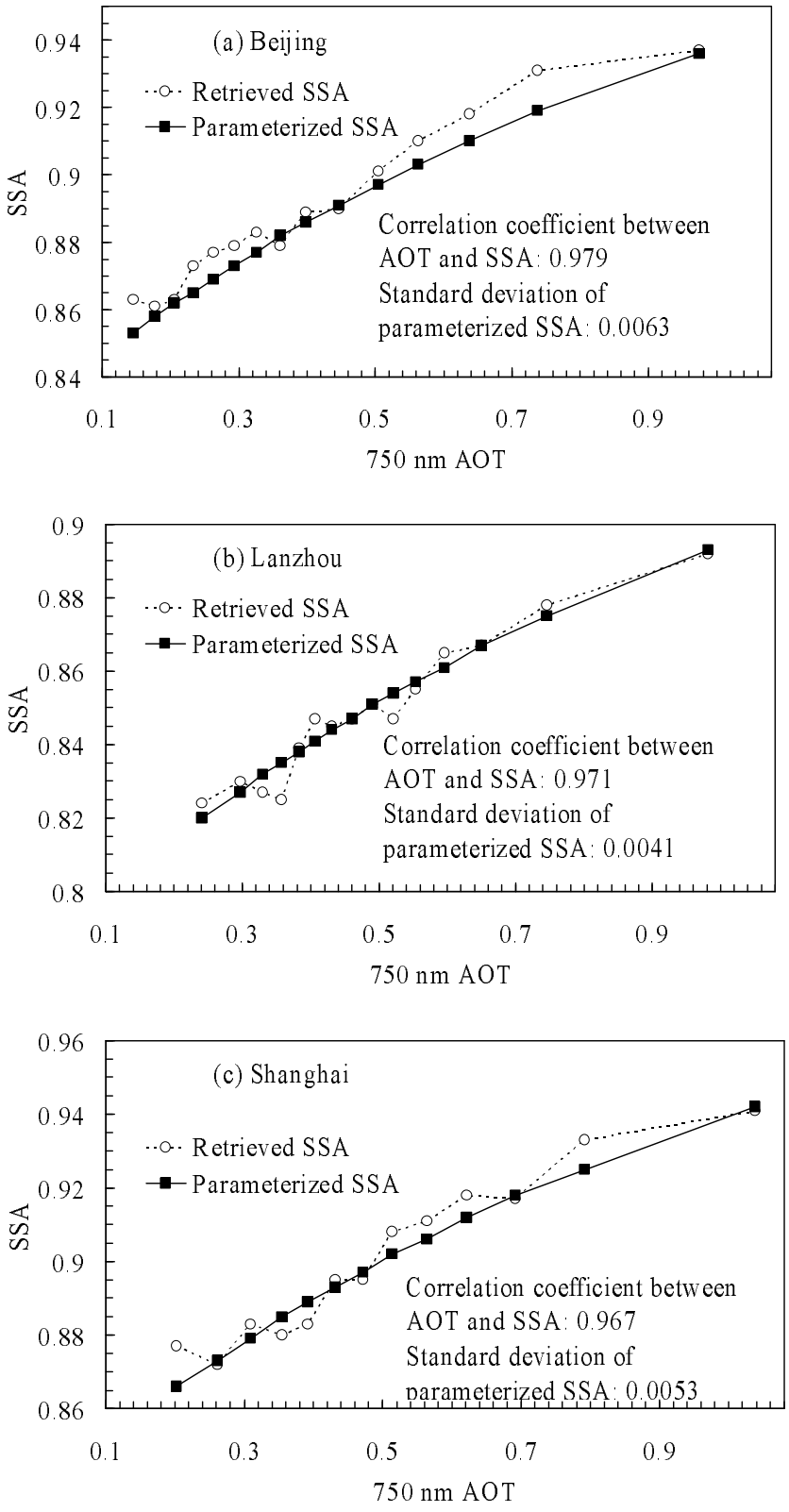

Fig. 4. Sub-mean SSA versus 750-nm AOT.

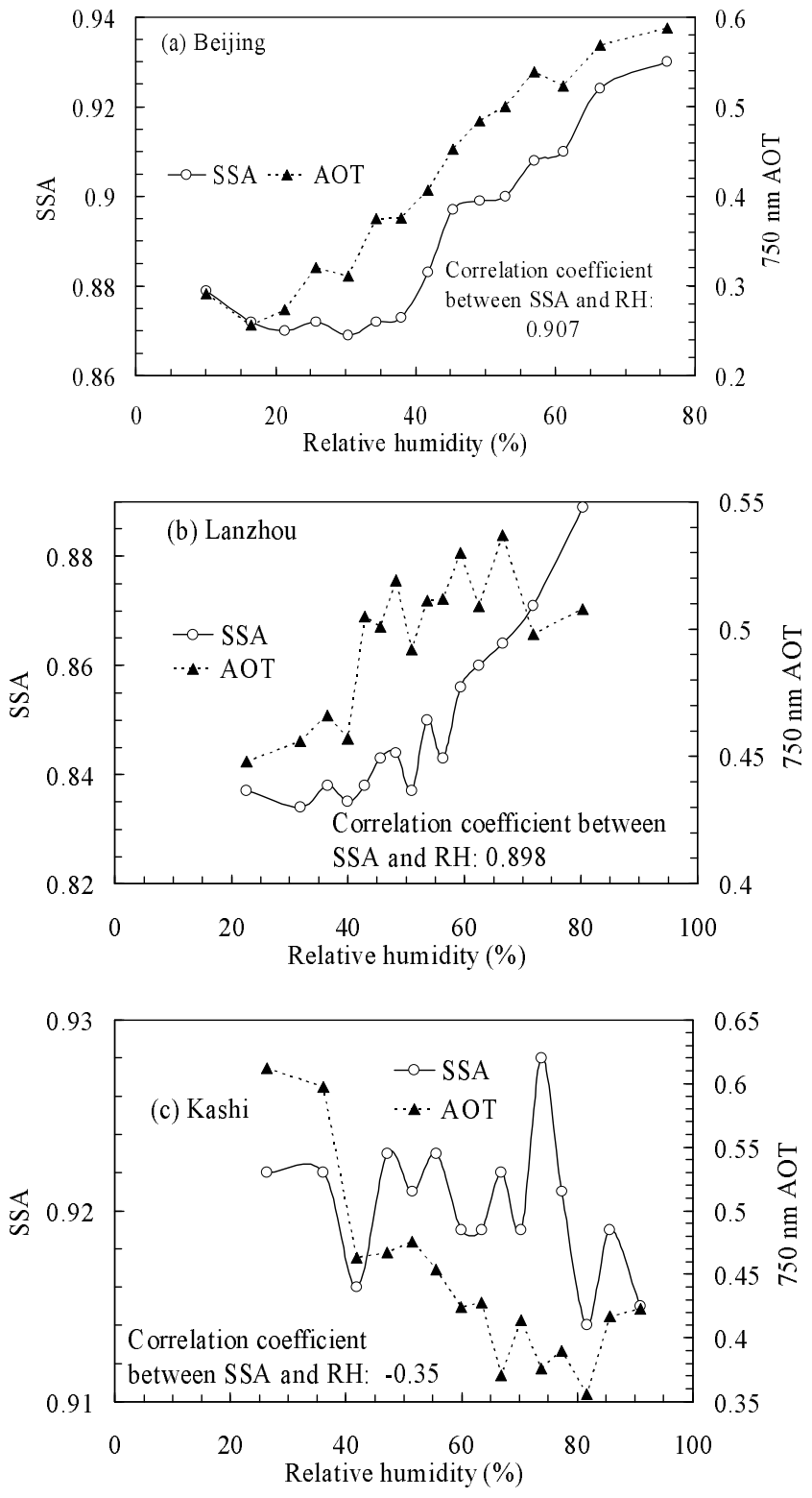

Fig. 5. Variation of SSA with RH and AOT.

Table 5. Correlation coefficients (η_1) between SSA and AOT, and correlation coefficient (η_2) between SSA and surface RH, parameterization coefficients a_1 and a_2, the standard deviation ($\delta_{\rm RMS}$) of sub-mean parameterized SSA, the mean deviation ($\delta_{\rm mean}$) of parameterized-SSA, and mean RH during 1998–2003.

Site	η_1	η_2	a_1	a_2	$\delta_{\rm RMS}$	$\delta_{\rm Mean}$	RH (%)
Shenyang	0.862	0.807	0.977	−0.14	0.0084	−0.00002	57.9
Beijing	0.979	0.907	1	−0.17	0.0063	−0.00495	53.8
Ejin Qi	0.632	0.744	0.965	−0.077	0.0050	−0.00001	32.2
Ürümqi	0.879	−0.237	0.934	−0.066	0.0043	−0.00001	57.2
Kashi	0.914	−0.35	0.998	−0.118	0.0055	0.00000	47.8
Golmud	0.848	0.384	1.03	−0.184	0.0101	0.00000	31.6
Lanzhou	0.971	0.898	0.959	−0.178	0.0041	0.00000	49.3
Zhengzhou	0.937	0.945	0.997	−0.13	0.0049	−0.00005	62.3
Shanghai	0.967	0.513	1	−0.165	0.0053	−0.00203	73.9
Wuhan	0.867	0.796	0.995	−0.088	0.0046	−0.00002	72.1
Chengdu	0.863	0.451	0.944	−0.075	0.0068	0.00000	75.0

trend of SSA with AOT. Based on this trend, the relationship between SSA and AOT is approximately parameterized as a function of AOT, given by:

$$\omega_{\rm a}(\lambda_0) = a_1 + a_2 \exp[-\tau_{\rm a}(\lambda_0)] \,, \qquad (7)$$

where $\omega(\lambda_0)$ is the SSA at the 750-nm wavelength (λ_0), and $\tau_{\rm a}(\lambda_0)$ is the λ_0-wavelength AOT. The two coefficients a_1 and a_2 are determined using the least square technique. Table 5 shows the two coefficients a_1 and a_2, means and standard deviations of mean parameterized SSA. As shown in Table 5, standard deviations of the parameterized sub-mean SSA are within 0.0101 in all 11 sites. The mean deviation ($\delta_{\rm Mean}$) is within ±0.00495 in all sites, showing a satisfactory accuracy of the parameterized SSA model.

Figure 4 illustrates variation of sub-mean SSA with 750-nm AOT for Beijing (Fig. 4a), Lanzhou (Fig. 4b) and Shanghai (Fig. 4c). As illustrated, SSA increases considerably when AOT enlarges for all three sites. In the case of Beijing, SSA increases (from 0.863 to 0.937) by an order of magnitude of around 0.074 when AOT changes from 0.145 to 0.974. There is also a SSA increase of about 0.07 when AOT increases at Lanzhou and Shanghai (Figs. 4b and 4c). The correlation coefficients between SSA and AOT are 0.979, 0.971 and 0.967 for Beijing, Lanzhou and Shanghai, respectively. The standard deviation of parameterized SSA is within 0.0063, showing a good agreement.

Looking again at Table 5, the correlation coefficient (η_2) between SSA and RH is negative over two sites (Ürümqi and Kashi), but it is positive (> 0.38) over the other eight sites. As shown in Fig. 5, there are two different variation trends of SSA with RH. Over the two sites of Beijing and Lanzhou, SSA variation with RH is small (< 0.01) when RH is less than 40%, but SSA evidently increases when RH is greater than 40%. In the case of the Kashi site, the situation is the reverse; where the trend is for SSA to decrease with RH. As pointed out by Paltridge and Platt (1976), when RH increases, real and imaginary parts of the refractive index of water-soluble aerosols tend to decrease, which should result in a larger SSA. This is considered as a significant impacting factor of the SSA increasing trend with RH in sites such as Beijing and Lanzhou. It can also be seen from Fig. 5 that the AOT in Beijing and Lanzhou increases with RH, when RH is less than 66%. However, the AOT in Kash has a decreasing trend with RH, which may be responsible for the negative correlation between SSA and RH.

4. Conclusions

The main conclusions of this study can be summarized as follows:

(1) A BRM to retrieve AIP and broadband (440–1020 nm) mean SSA has been developed, and four sets of SSA selection criteria have been proposed. Satisfactory agreement of BRM SSA with AERONET SSA at the Beijing site was found. The difference between both mean SSA values is less than 0.02.

(2) The annual mean SSA changes from 0.941 (Wuhan) to 0.849 (Lanzhou), and the AIP from 0.0054 to 0.0203. The 11-site mean annual mean SSA and AIP are 0.898 and 0.0119, respectively. The SSA during winter is smaller for most sites.

(3) It is interesting that the trend is for SSA to considerably increase when AOT enlarges. In the case of Beijing, the increasing magnitude is up to 0.074.

(4) SSA increases when RH increases for most sites, but the trend is for it to decrease over some sites (Kashi and Ürümqi) in the west of northern China.

Acknowledgements. This work was supported by the National Basic Research Program of China (Grant No. 2006CB403702), the National Natural Science Foundation of China (Grant Nos. 40333029, and 40475014). The au-

thors acknowledge the use of data of the AERONET site in Beijing. Thanks are extended to PI Hong Bin Chen and Philippe Goloub for their effect in establishing and maintaining the AERONET site.

REFERENCES

Bengtsson, L., E. Roeckner, and M. Stendel, 1999: Why is the global warming proceeding much slower than expected. *J. Geophys. Res.*, **104**, 3865–3878.

Charlson, R. J., S. E. Schwartz, J. M. Hales, R. D. Cess, J. A. Coakley, Jr. J. E. Hansen, and D. J. Hofmann, 1992: Climate forcing by anthropogenic aerosols. *Science*, **255**, 423–429.

CMA (China Meteorological Administration), 1996: *Meteorological Radiation Observation Method.* China Meteorological Press, Beijing, 165pp.

Dubovik, O., B. N. Holben, T. F. Eck, A. Smirnov, Y. J. Kaufman, M. D. King, D. Tanre, and I. Slutsker, 2002: Variability of absorption and optical properties of key aerosol types observed in worldwide locations. *J. Atmos. Sci.*, **59**, 590–608.

Eck, T. F., and Coauthors, 2005: Columnar aerosol optical properties of AERONET sites in central eastern Asia and aerosol transport to the tropical mid-Pacific. *J. Geophys. Res.*, **110**, D06202, doi:10,1029/2004JD005274.

Hartley, W. S., P. V. Hobbs, J. L. Ross, P. B. Ressell, and J. M. Livingston, 2000: Properties of aerosol aloft relevant to direct radiative forcing off the mid-Atlantic coast of the United States. *J. Geophys. Res.*, **105**, 9859–9885.

Herman, B. M., S. R. Browning, and J. J. De Luisi, 1975: Determination of the effective imaginary term of the complex refractive index of atmospheric dust by remote sensing: The Diffuse-Direct radiation method. *J. Atmos. Sci.*, **32**, 918–925.

Holben, B. N., and Coauthors, 1998: AERONET—A federated instrument network and data archive for aerosol characterization. *Remote Sens. Environ.*, **66**, 1–16.

Kaufman, Y. J., and Coauthors, 1997: Passive remote sensing of tropospheric aerosol and atmospheric correction for the aerosol effect. *J. Geophys. Res.*, **102**, 16815–16830.

Kiehl, J. T., and B. P. Briegleb, 1993: The radiative role of sulfate aerosols and greenhouse gases in climate forcing. *Science*, **260**, 311–314.

Menon, S., J. Hansen, L., Nazarenko, and Y. Luo, 2002: Climate effects of black carbon aerosols in China and India. *Science*, **297**, 2250–2253.

Nakajima, T., T. Hayasaka, A. Higrashi, G. Hashida, N. Moharram-Nejad, N. Yahya, and V. Hamzeh, 1996: Aerosol optical properties in the Iranian region obtained by ground-based solar radiation measurements in the summer of 1991. *J. Appl. Meteor.*, **35**, 1265–1278.

Paltridge, G. W., and C. M. R. Platt, 1976: *Radiative Processes in Meteorology and Climatology.* Elsevier Science, 318pp.

Penner, J. E., and Coauthors, 1994: Quantifying and minimizing uncertainty of climate forcing by anthropogenic aerosols. *Bull. Amer. Meteor. Soc.*, **75**, 375–400.

Qiu, J., 2001: Broadband extinction method to determine atmospheric aerosol optical properties. *Tellus*, **53B**, 72–82.

Qiu, J., 2003: Broadband extinction method to determine aerosol optical depth from accumulated solar direct radiation. *J. Appl. Meteor.*, **42**, 1611–1625.

Qiu, J., 2006: Broadband diffuse radiation method to retrieve radiation-weighted mean aerosol single scattering albedo. *Chinese J. Atmos. Sci.*, **30**, 767–777. (in Chinese)

Qiu, J., L. Yang, and X. Zhang, 2004: Characteristics of imaginary part and single scattering albedo of urban aerosol in northern China. *Tellus*, **56B**, 276–284.

Qiu, J., X. Zong, and X. Zhang, 2005: A study of the scaling height of the tropospheric aerosol and its extinction coefficient profilre. *Journal of Aerosol Science*, **36**, 361–371.

Taylor, K. E., and J. E. Penner, 1994: Response of the climate system to atmospheric aerosols and greenhouse gases. *Nature*, **369**, 734–737.

Tegen, I., A. A. Lasis, and I. Fung, 1996: The influence of mineral aerosols from disturbed soils on the global radiation budget. *Nature*, **380**, 419–422.

Wei, D., and J. Qiu, 1998: Wideband method to retrieve the imaginary part of complex refractive index of atmospheric aerosols, Part I: Theory. *Chinese J. Atmos. Sci.*, **22**, 677–685. (in Chinese)